Brodogradnja Volume 77 Number 3 (2026) 77306

University of Zagreb
Faculty of Mechanical
Engineering and Naval
Architecture

journal homepage: www.brodogradnja.fsb.hr

Brodogradnja

An International Journal of Naval Architecture and
Ocean Engineering for Research and Development

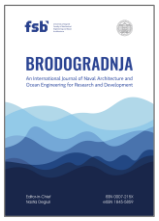

Toughness strengthening method of course changing control for ships based on nonlinear modification

Haoyang Yu[1,2], *Xianku Zhang*[1,2*], *Haoyun Tang*[1,2]

[1]*Navigation College,Dalian Maritime University, 1 Linghai road, Dalian, 116026, China*
[2]*State Key Laboratory of Maritime Technology and Safety, Dalian Maritime University, 1 Linghai road, Dalian, 116026, China*

ARTICLE INFO

Keywords:
Closed-loop gain shaping algorithm (CGSA)
Nonlinear modification
Zero-order holder (ZOH)
Positive feedback
Automatic switching control

ABSTRACT

To enhance the resilience of ship course-keeping and large-angle collision-avoidance maneuvers under cyberattacks, this study proposes a cyber-resilient course control methodology based on an innovative feedback-switching architecture. A dual-feedback automatic switching mechanism that integrates both positive and negative feedback modes is proposed. In this framework, sign inversion of measurement signals induced by simulated cyberattacks are interpreted as positive feedback, enabling automatic switching between positive and negative feedback. This transforms the large-angle collision avoidance task into a small-angle course deviation problem. The core design employs a second-order closed-loop gain-shaping algorithm to synthesize a robust linear controller, which is further augmented with a sine-based nonlinear compensator and implemented via zero-order hold. Compared with conventional designs, the combined approach reduces actuator amplitude by 41.7% reduction and rudder actuation frequency by 33.2%. Closed-loop stability is established through description–function analysis and verified via the Nyquist stability criterion. Full-scale simulations on the "Yupeng" training vessel under standard sea conditions demonstrate that the integrated system maintains course-keeping accuracy within 0.8° during signal-inversion attacks while reducing steering energy consumption by 18.6%. The proposed automatic switching architecture effectively mitigates cyberattack effects during large-angle evasive maneuvers, reduces actuator wear and energy consumption, and enhances the safety and reliability of intelligent ships.

1. Introduction

1.1 Background

The rapid development of trade globalization has established maritime transport as a dominant force in international trade. The shipping industry handles approximately 17% of the global freight volume and contributes to over 50% of total trade turnover [1], highlighting its pivotal role in global supply chains.

* Corresponding author.
E-mail address: zenghong@dlmu.edu.cn

https://doi.org/10.21278/brod77306
Received 14 March 2025; Received in revised 4 October 2025; Accepted 16 October 2025
Available online 26 December 2025
ISSN 0007-215X; eISSN 1845-5859

Therefore, the navigational safety and operational efficiency of ships, as the primary means of maritime transportation, have garnered increasing attention. Concurrently, the rapid advancement of network technologies has propelled shipping into an era of informatization and intelligence. The development of intelligent ships and increasing autonomy levels have introduced unprecedented efficiency and convenience to the shipping industry [2]. The deep integration of cyber–physical systems (CPS) in ship motion control [3] provides powerful solutions to traditional challenges in course-keeping and collision avoidance; however, it introduces new security challenges [4].

Cyberattacks on maritime transportation systems have become increasingly frequent, posing serious threats to navigational safety. Vulnerabilities in network communications significantly increase ship exposure to diverse cyber threats, where attackers can employ various means, including ransomware, false data injection (FDI), GPS jamming and spoofing, denial-of-service (DoS) attacks, malware propagation, and phishing, to compromise vessel systems [5-10]. Among these attack vectors, signal inversion attacks—malicious alterations or accidental reversals of sensor signal polarity—represent a particularly significant threat. This form of attack can be actively executed by hackers, for instance, by intruding into sensor network nodes or data buses to invert the polarity of transmitted signal values; or it can occur unintentionally during system navigation and maintenance owing to operator errors, such as incorrect wiring leading to line reversal. Despite its seemingly simple mechanism, the impact is severe, as it fundamentally undermines the core assumption of negative feedback control systems—that feedback signals accurately represent the controlled variable's state. This type of attack can be regarded as an extreme and easily implementable form of FDI [11], potentially resulting in incorrect heading signals that cause yaw deviation and inaccurate positional data resulting in collisions [12], thereby severely compromising the safety and reliability of the entire shipping system [13]. This study addresses this covert yet highly detrimental practical threat by developing resilient control strategies.

However, traditional course control algorithms, such as proportional-integral-derivative (PID) control, often exhibit insufficient resilience when confronted with strong uncertainties and nonlinearities introduced by such cyber-attacks [14]. Furthermore, during emergency scenarios requiring large-angle collision avoidance maneuvers, conventional methods are slow and time-consuming, causing frequent rudder movements and significantly increasing energy consumption and mechanical wear. Therefore, developing an intelligent and resilient control strategy capable of counteract cyberattacks, particularly signal inversion attacks, while enabling rapid, stable large-angle course changes and maintaining energy efficiency is essential for ensuring the navigational safety of intelligent ships. This remains a critical and urgent challenge in the field.

1.2 Related work

Numerous schemes have been proposed to enhance the performance and efficiency of control strategies. Ma [15] integrated a zero-order holder to reduce rudder frequency and amplitude, thereby lowering energy usage. Zhang [16] proposed an active disturbance rejection control algorithm to further improve energy efficiency and reduce carbon emissions. Gao [17] addressed course-keeping and energy-saving challenges for unstable large oil tankers by incorporating a swish function into a nonlinear feedback loop, with experimental results validating its effectiveness. Additional contributions include those of Li [18], who enhanced longitudinal stabilization by integrating a nonlinear feedback switch with a third-order closed-loop gain-shaping algorithm [19]; Islam [20], who introduced robust integral backstepping, cooperative, and terminal cooperative controllers; and He [21], who developed a finite-time course-keeping controller. Furthermore, Li [22] presented a method that integrates conditional judgments with nonlinear feedback to minimize energy consumption during course control.

To address cybersecurity challenges, existing research has largely focused on constructing external defense mechanisms or compensating for specific attacks. For example, Song [23] designed a fuzzy state observer combined with a fuzzy mixed-triggered dynamic positioning (DP) output controller; simulations confirmed its feasibility and superiority. Ding [24] developed a point-output sampling control strategy based on limited measurable outputs and Lyapunov functions to demonstrate effective energy conservation and

carbon reduction. Zhou [25] improved ship safety during cyberattacks using an integrated safety security approach based on a systems theoretic process analysis (STPA). Guo [26] proposed a cloud-computing-based real-time risk detection and protection framework that employs multisensor nodes to analyze data for malicious activity and automatically execute protective measures.

Nevertheless, a review of the existing literature reveals certain notable limitations. Most efforts focus on performance optimization in conventional scenarios or external security measures, with limited exploration of the intrinsic resilience mechanisms within control systems. Specifically, the prevailing control strategies predominantly rely on negative feedback frameworks that assume sensor signal accuracy, rendering them critically vulnerable to fundamental attacks, such as signal inversion. Although certain studies have begun to address control under cyberthreats, their attack models have primarily focused on FDI or DoS attacks, paying insufficient attention to the modeling and implications of more covert and disruptive signal polarity inversion attacks. Moreover, existing approaches often depend on external detection and post-factum compensation, lacking dynamic reconfiguration capabilities embedded within the control algorithm for autonomous mode switching to effectively neutralize attacks. The absence of inherent resilience within the control strategy constitutes a significant vulnerability for intelligent ships confronting complex cyber threats.

1.3 Contributions

To address these limitations, this study proposes a novel cyber-resilient course control strategy that integrates automatic positive–negative feedback switching with nonlinear modification and a zero-order holder. The main contributions are as follows:

(1) An automatic switching mechanism was established by employing positive feedback to simulate cyberattacks via erroneous sensor measurements. The mechanism significantly enhanced the resilience and reliability of the course-keeping control system, providing both technical support and a theoretical framework for intelligent-ship development.

(2) An automatic switching control algorithm was proposed for large-angle course changes that enhances collision-avoidance performance as well as reduces energy consumption during maneuvers and decreases rudder wear.

(3) A control system was designed that integrates nonlinear modifications with a zero-order holder. Simulation experiments verify that this combination effectively achieves energy conservation, carbon reduction, and green environmental objectives for intelligent ships.

2. Controller design using nonlinear modification, closed-loop gain shaping algorithm (CGSA), and zero-order holder (ZOH)

2.1 Mathematical model of ship motion

In studies on ship course control systems, the mathematical modeling of ship motion typically begins with a linear Nomoto model:

$$\ddot{\psi}+\frac{1}{T_0}\dot{\psi}=\frac{K_0}{T_0}\delta \tag{1}$$

where ψ represents the heading angle, $\dot{\psi}$ is the first derivative of ψ , $\ddot{\psi}$ is the second derivative of ψ , K_0 and T_0 are the ship motion maneuverability indices, and δ is the rudder angle.

However, this model is idealized and deviates significantly from the actual dynamics of ship motion. To develop a data model that better aligns with real ship dynamics and enhances the model's fidelity to the actual motion process, this study introduces a nonlinear term $\left(K_0/T_0\right)H\left(\dot{\psi}\right)$ to replace $\left(\dot{\psi}/T_0\right)$, which is expressed as follows:

$$H\left(\dot{\psi}\right)=\alpha\dot{\psi}+\beta\dot{\psi}^3 \tag{2}$$

where α and β are the proportional coefficients of the first and third powers of the yaw rate, respectively; these coefficients can be determined using the least squares method.

Thus, the nonlinear second-order model of the ship motion response is formulated as follows:

$$\ddot{\psi}+\frac{K_0}{T_0}\left(\alpha\dot{\psi}+\beta\dot{\psi}^3\right)=\frac{K_0}{T_0}\delta \tag{3}$$

Eq. (3) is the mathematical model used for the system simulation, whereas the simplified transfer function form of the Nomoto model used for the linear controller design is expressed as follows:

$$G_{\psi\delta}(s)=\frac{\psi}{\delta}=\frac{K_0}{s\left(T_0 s+1\right)} \tag{4}$$

2.2 Linear controller design

In 1998, Zhang [27] introduced the closed-loop gain-shaping algorithm, a robust control strategy that integrates control theory with loop shaping. This algorithm is designed for streamlined engineering implementation and serves as a simplified approach for achieving robustness in control systems. Fig. 1 shows the standard structure of closed-loop gain shaping, where r represents the set course direction, u is the control input, d represents the wave and wind disturbances, and y is the output.

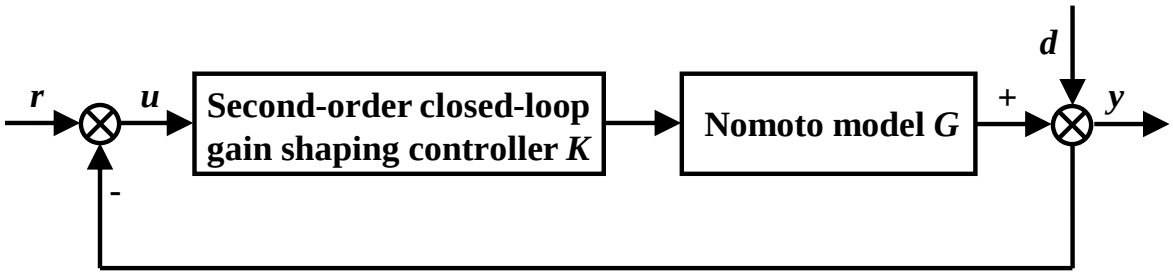

Fig. 1 Standard structure chart of closed-loop gain shaping

By utilizing the relationship between the complementary sensitivity functions T and S (i.e., $S=1-T$), the sensitivity function S can be formulated indirectly, thereby enabling the inverse derivation of the control law K.

Furthermore, the sensitivity function $S=1/(1+GK)$ represents the closed-loop transfer function mapping disturbances d to the output y, whereas the complementary sensitivity function $T=GK/(1+GK)$ describes the closed-loop transfer function from the reference inputs r to the output y.

Fig. 2 presents the characteristic profile of the $S\&T$ singular value curve. To maintain robust stability in control systems, the closed-loop frequency spectrum should exhibit adequate transmission characteristics at lower frequencies. Furthermore, proper configuration of the maximum singular value at unity magnitude is essential for achieving accurate reference signal tracking while eliminating steady-state errors. Bandwidth frequency is essential in defining the dynamic performance of a control system. Meanwhile, the attenuation gradient of the frequency spectrum directly determines the disturbance rejection capability; a more pronounced roll-off rate corresponds to an improved suppression of external disturbances and measurement noise. However, an overly steep closing slope increases the controller's order, complicating implementation. In practice, closing slopes are generally chosen as -20 dB/dec, -40 dB/dec, or -60 dB/dec.

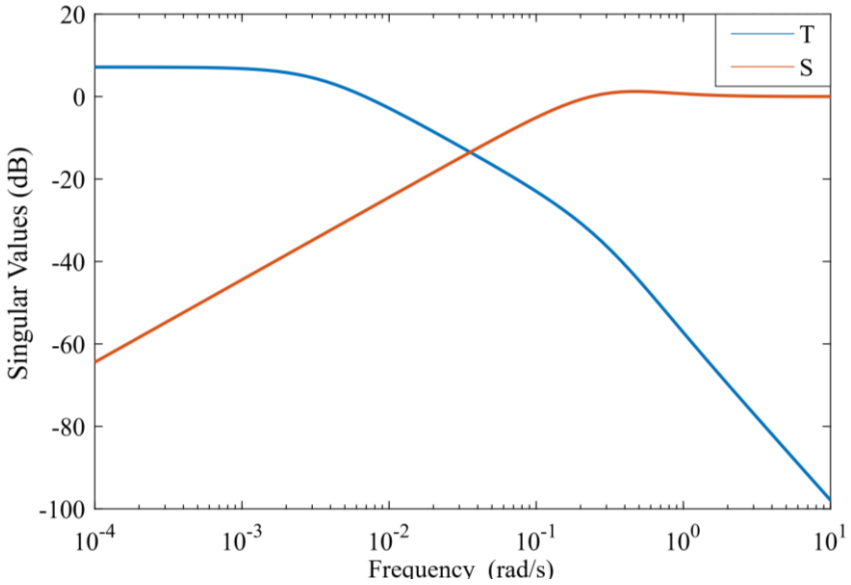

Fig. 2 Typical S & T singular value curve

Based on Eq. (4) and the closed-loop gain-shaping algorithm, the following relationship holds:

$$\frac{1}{\left(T_1 s+1\right)^2}=\frac{G(s)K(s)}{1+G(s)K(s)} \tag{5}$$

$$K(s)=\frac{1}{GT_1 s\left(T_1 s+2\right)} \tag{6}$$

By incorporating the Nomoto model, the control law can be derived as follows:

$$K(s)=\left(\frac{T_0}{K_0 T_1}s+\frac{1}{K_0 T_1}\right)\frac{1}{T_1 s+2} \tag{7}$$

A constant ρ is selected within the PD controller [28]. If ρ is chosen within the range 1–10, the system can significantly reduce its dynamic response time without impacting stability. For this study, a value of $\rho=4$ is employed. To eliminate static error in the system when using the CGSA controller design approach, a small constant term ε can be added to the denominator of the model's transfer function to consider the effect of an uncertain constant disturbance on the ship [29]. In this study, the constant is selected as $\varepsilon=0.005$. Consequently, the traditional Nomoto model is expressed as follows:

$$G_1(s)=\frac{K_0}{s\left(T_0 s+1\right)+\varepsilon} \tag{8}$$

The controller selected in this study is K_c, and the control law can be provided by the following relation:

$$K_c(s)=\left(\frac{T_0}{K_0 T_1}s+\frac{1}{K_0 T_1}+\rho+\frac{\varepsilon}{K_0 T_1 s}\right)\frac{1}{T_1 s+2} \tag{9}$$

2.3 System stability analysis

The Lyapunov stability analysis method is widely used to evaluate the stability of course-keeping controllers within the CGSA architecture. However, the implementation of this theoretical framework in the present control system mandates the construction and numerical solution of positive-definite real symmetric matrices, a process characterized by mathematical complexity and operational abstraction. To address these

computational challenges, we adopted the Nyquist stability criterion from frequency-domain analysis techniques to verify controller stability. By integrating Nomoto's ship dynamics model with the governing Eqs. (9), the open-loop transfer function of the control system can be mathematically established as follows:

$$\begin{aligned} G(s) &= G_1(s)K_c \\ &= \frac{T_0 s^2 + s + \rho K_0 T_1 s + \varepsilon}{K_0 T_1 s} \frac{1}{T_1 s + 2} \frac{K_0}{s(T_0 s + 1) + \varepsilon} \\ &= \frac{T_0 s^2 + s + \rho K_0 T_1 s + \varepsilon}{T_1 s(T_1 s + 2)\left[s(T_0 s + 1) + \varepsilon\right]} \\ &= \frac{1/T_1^2 \left[s^2 + s(1 + \rho K_0 T_1)/T_0 + \varepsilon/T_0\right]}{s(s + 2/T_1)\left[s + \left(1 + \sqrt{1 - 4T_0\varepsilon}\right)/2T_0\right]\left[s + \left(1 - \sqrt{1 - 4T_0\varepsilon}\right)/2T_0\right]} \end{aligned} \tag{10}$$

This study defines $s = jw$; consequently, the open-loop frequency response can be expressed as:

$$G(jw) = \frac{1/T_1^2 \left[(jw)^2 + jw(1 + \rho K_0 T_1)/T_0 + \varepsilon/T_0\right]}{jw(jw + 2/T_1)\left[jw + \left(1 + \sqrt{1 - 4T_0\varepsilon}\right)/2T_0\right]\left[jw + \left(1 - \sqrt{1 - 4T_0\varepsilon}\right)/2T_0\right]} \tag{11}$$

The open-loop poles are $p_1 = -2/T_1$, $p_2 = -\left(1 + \sqrt{1 - 4T_0\varepsilon}\right)/2T_0$, $p_3 = -\left(1 - \sqrt{1 - 4T_0\varepsilon}\right)/2T_0$. The corresponding Nyquist plot is depicted in Fig. 3. Let N denote the number of encirclements around the Nyquist plot at the point $(-1, j_0)$, where a clockwise rotation is considered negative and a counterclockwise rotation positive. Let P and Z represent the number of poles of the open-loop and closed-loop transfer functions in the right half of the $G(s)$ plane, respectively. According to the Nyquist stability criterion, the following relationship holds:

$$Z = P - N \tag{12}$$

If $Z = 0$ is used, the closed-loop system is stable. The open-loop transfer function $G(s)$ contains no poles in the right-half of the complex plane (Fig. 3). The Nyquist locus $G(jw)$ exhibits zero net encirclement at the critical point. Applying the Nyquist stability criterion to $P = 0$ and $N = 0$ yields $Z = P - N = 0$. Specifically, the closed-loop characteristic equation has no zeros in the RHP. Therefore, under the stated assumptions, the closed-loop system contains no right half-plane poles and is asymptotically stable.

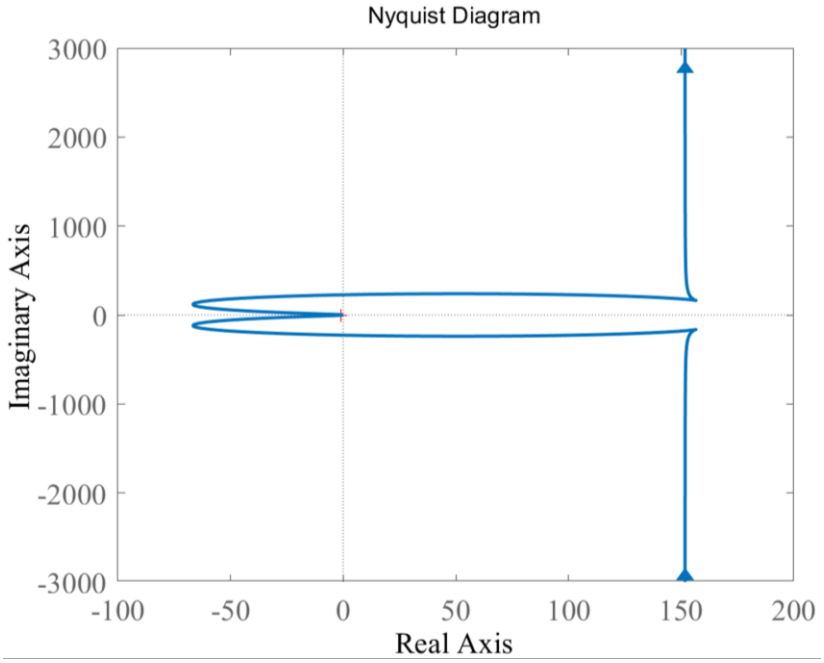

Fig. 3 Nyquist plot

2.4 Robustness analysis

The parametric perturbation configurations inherent to the closed-loop gain-shaping algorithm (CGSA) are then systematically investigated. By combining the small-gain theorem principles with H_∞ mixed-sensitivity algorithm, we formally established the foundational disturbance model for this control framework.

The canonical H_∞ control configuration shown in Fig. 4 demonstrates the systematic incorporation of disturbance dynamics through nonlinear operator compositions. This integration preserves the stability margins and robustness specifications during H_∞ controller engagement. The initial analysis applies small-gain criteria to the classical H_∞ control topology, yielding a critical relationship between plant perturbations and closed-loop transfer operators, as mathematically expressed in Eq. (13):

$$\left\| GK/\left(1+GK\right)\Delta \right\|_\infty = \left\| T\Delta \right\|_\infty < 1 \tag{13}$$

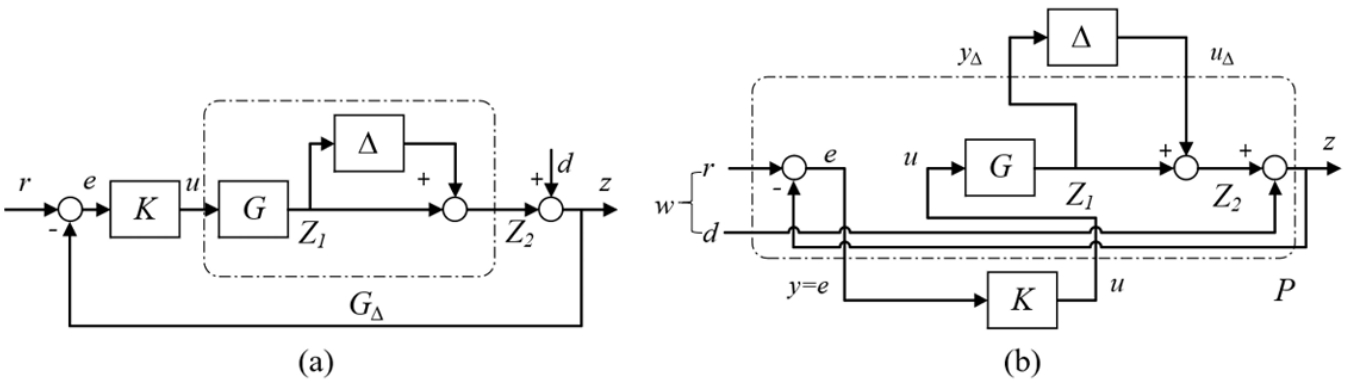

Fig. 4 A typical H_∞ control problem

Eq. (13) reveals two fundamental characteristics: (i) bounded magnitude modulation of process model uncertainties Δ , and (ii) regulated closed-loop gain confinement $GK/\left(1+GK\right)$ that guarantees Lyapunov-type stability preservation.

Considering Fig. 1 and the characteristics of CGSA, the following results were obtained:

$$\begin{aligned} &\|T\|_\infty \bullet \|S\|_\infty < 1 \\ &\|TS\|_\infty < 1 \end{aligned} \tag{14}$$

Using Eq. (13) and Eq. (14), we derive:

$$\|\Delta\|_\infty = \|S\|_\infty = \|1-T\|_\infty \tag{15}$$

Based on Eq. (15), the model disturbance form of CGSA is similar to that of the sensitivity function S and must satisfy the following conditions: $\|\Delta\|_\infty < 1$.

The theoretical foundation of the CGSA is derived from singular value characterization through weighting function optimization in H_∞ robust control theory. Consequently, structured uncertainty modeling is inherently integrated into the design process, with robust stability rigorously verified via analytical proofs. Our findings from the small-gain analysis and H_∞ mixed-sensitivity paradigms confirm that the CGSA's admissible perturbation bounds maintain functional congruence with the sensitivity function S. This critical correspondence determines the maximum allowable modeling discrepancies when engineering robust controllers using CGSA methodologies [30].

2.5 Design of zero-order holder for reducing rudder frequency

Owing to the zero-order holder (ZOH)'s tendency for rapid amplitude attenuation at higher frequencies, it effectively functions as a low-pass filter, rendering it well suited to the low-frequency nature of ship control signals. Moreover, the ZOH reduced the steering frequency, thereby protecting the steering mechanism from wear. Consequently, ZOH is incorporated into the controller.

The ZOH operates by holding the sampled signal for a specified period prior to resampling. When implemented in the rudder roll damping controller, it maintains signal continuity between the controller and rudder actuator and reduces the rudder oscillation frequency to an acceptable level. The mathematical description of ZOH is as follows:

$$e(nT + \Delta t) = e(nT) \tag{16}$$

where T represents the hold time of the zero-order holder and e denotes the course error (i.e., the difference between the setting and actual course), typically expressed as $e = \psi_r - \psi$ in Eq. (16). This indicates that the course error remains constant within each sampling period; specifically, it remains steady from time nT to $nT + \Delta t$ and is updated only at the next sampling instant, $(n+1)T$.

The nonlinear Nomoto ship model, including the ZOH component, is established as follows:

$$G_2(s) = \frac{K_0\left(1-e^{-Ts}\right)}{s(T_0 s+1)} \tag{17}$$

Subsequently, the Taylor series expansion of $\left(1-e^{-Ts}\right)/s$ is performed and retain terms up to the first order are retained:

$$\frac{1-e^{-Ts}}{s} = \frac{1}{s}\left(1-\frac{1}{e^{Ts}}\right) \approx \frac{T}{1+Ts} \tag{18}$$

Eq. (18) is substituted into Eq. (17):

$$G_2(s) \approx \frac{K_0 T}{(T_0 s+1)(1+Ts)} \tag{19}$$

Let Ω represent the open right-half plane and let $W_2(s)S_2(s)$ denote the transfer function from the normalized disturbance to the system output:

$$\begin{aligned}&\left\|W_2(s)S_2(s)\right\|_\infty \\ &=\left\|W_2(s)\left[1-G_2(s)Q_2(s)\right]\right\|_\infty \\ &=\sup_{\mathrm{Re}s>0}\left|W_2(s)\left[1-G_2(s)Q_2(s)\right]\right|\end{aligned} \tag{20}$$

Let $W_2(s)$ be set to $1/s$; then, the minimum value of $\left\|W_2(s)S_2(s)\right\|_\infty$ must asymptotically converge:

$$\lim_{s\to 0}S_2(s)=\lim_{s\to 0}\left[1-G_2(s)Q_2(s)\right]=0 \tag{21}$$

2.6 Nonlinear modification function design and stability analysis

In this study, a nonlinear modification driven by the sine function shown in Eq. (22) is added to the system, representing the input to the control system:

$$f(u)=\sin(\omega u) \tag{22}$$

A block diagram of the control system after introducing the nonlinear modification link is shown in Fig. 5.

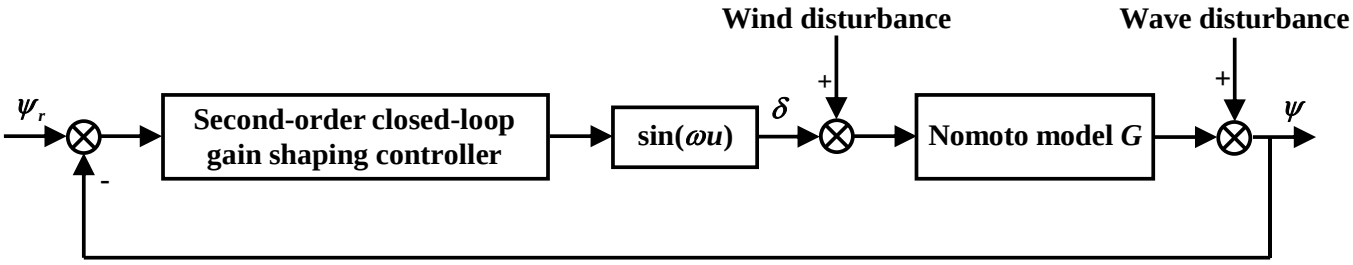

Fig. 5 System control diagram based on nonlinear sine function modification

The control law, incorporating nonlinear modifications, is a form of nonlinear control. The subsequent section employs the terminal value theorem to illustrate the impact of the nonlinear modification on the original system.

The stability assessment of second-order closed-loop configurations in maritime systems fundamentally requires positive temporal constant parameters, which are inherent characteristics of marine control implementations. For sinusoidally modified nonlinear control architectures, an analytical evaluation combined the final value theorem with the closed-loop gain-shaping methodology of robust control [31]. This dual analytical approach yields the following stability verification framework.

(1) Effect on the steady-state behavior of the closed-loop system: Let the reference input signal be a step signal with amplitude ψ_r. The impact of the nonlinear modification on static performance is analyzed under the condition that the change in the original control output u is sufficiently small, such that $\sin(\omega u)\approx\omega u$ (the maximum rudder angle is 35°, equivalent to 0.61 rad, which is considered small). For simplicity, the linear ship motion model was defined as $G_1=K_0/\left[s(T_0s+1)+\varepsilon\right]$. The steady-state output heading angle ψ of the system was obtained directly using the final value theorem, as follows:

$$
\begin{aligned}
\psi(\infty) &= \lim_{s\to 0} s \frac{G_1 K_c \omega}{1+G_1 K_c \omega} \frac{\psi_r}{s} \\
&= \lim_{s\to 0} \frac{\dfrac{K_0}{s(T_0 s+1)+\varepsilon} \dfrac{1}{T_1 s+2}\left(\dfrac{T_0}{K_0 T_1} s+\dfrac{1}{K_0 T_1}+\rho+\dfrac{\varepsilon}{K_0 T_1 s}\right)\omega}{1+\dfrac{K_0}{s(T_0 s+1)+\varepsilon} \dfrac{1}{T_1 s+2}\left(\dfrac{T_0}{K_0 T_1} s+\dfrac{1}{K_0 T_1}+\rho+\dfrac{\varepsilon}{K_0 T_1 s}\right)\omega} \psi_r \\
&= \lim_{s\to 0} \frac{K_0 \omega\left(T_0 s^2+s+\rho K_0 T_1 s+\varepsilon\right)}{\left[s(T_0 s+1)+\varepsilon\right](T_1 s+2) K_0 T_1 s+K_0 \omega\left(T_0 s^2+s+\rho K_0 T_1 s+\varepsilon\right)} \psi_r \\
&= \lim_{s\to 0} \frac{K_0 \omega T_0 s^2+\left(1+\rho K_0 T_1\right) K_0 \omega s+K_0 \omega \varepsilon}{K_0 T_0 T_1^2 s^4+\left(T_1+2K_0\right) T_0 T_1 s^3+\left(2T_1+T_1^2 \varepsilon+\omega T_0\right) K_0 s^2+\left(2T_1 \varepsilon+\omega+\rho K_0 T_1 \omega\right) K_0 s+K_0 \omega \varepsilon} \psi_r \\
&= \frac{K_0 \omega \varepsilon}{K_0 \omega \varepsilon} \psi_r = \psi_r
\end{aligned}
\tag{23}
$$

Thus, the sine-based nonlinear control introduces no additional effect on the steady-state output error of the system.

(2) Impact on the closed-loop dynamic characteristics: The input–output relationship is mathematically described by the transfer function:

$$
\frac{\psi}{\psi_r} = \frac{G_1 K_c \omega}{1+G_1 K_c \omega} \tag{24}
$$

In marine course-keeping control systems, wave-induced disturbances are manifested as high-frequency excitations. The design parameter $\omega < 1$ was conventionally selected to exclude the dominant wave spectral components in high-frequency domains. Following H_∞ robust control principles, the open-loop transfer matrix $G_1 K_c$ demonstrates frequency-dependent gain attenuation, which is maximal in low-frequency operational bands and minimal in high-frequency regimes [32]. A comparative analysis of Eq. (24), and the closed-loop transfer function $G_1 K_c / (1+G_1 K_c)$ reveals negligible changes in dynamic performance, owing to the pronounced low-frequency amplification characteristics.

(3) Effect on the control output of the closed-loop system. The transfer function from the input ψ_r to the output δ of the system is:

$$
\frac{\delta}{\psi_r} = \frac{K_c \omega}{1+G_1 K_c \omega} \tag{25}
$$

An analysis method similar to that used in Eq. (24) indicates that the value of $K_c \omega$ decreases more significantly than that of $G_1 K_c \omega$. Thus, introducing ω can reduce the control output.

(4) However, $\sin(\omega u) \approx \omega u$ does not hold if e is considerably large. In this case, demonstrating the effects of sine-driven nonlinear control is challenging and falls outside the scope of this study.

3. Switching systems with positive and negative feedback controller design

3.1 Principle of automatic switching system for positive and negative feedback

The essence of the negative feedback control is to utilize the actual heading angle as a feedback signal, compare it with the setting course, and generate an error signal. By continuously adjusting the input, the error

between the heading angle and setting course is minimized, ultimately achieving optimal course-keeping control for the ship.

When the system experiences a signal-inversion attack, the feedback signal is erroneously modified such that it opposes the set course. Assuming that the desired feedback signal is y , the actual feedback signal after an attack is $y' = -y$. Negating the feedback signal adjusts it to $-y' = y$. At this point, the controller interprets this corrected feedback signal as normal, and the error calculation is expressed as:

$$e = r - (-y) = r + y \tag{26}$$

Thus, the feedback signal of the negative feedback system is restored to normal, enabling the system to execute the appropriate control actions to counteract the effects of an attack.

The PID controller generates its control output based on the error between the setting course and feedback signal, which is employed to adjust the motion of the ship to align with the setting course. During signal inversion, the controller issues a reverse command, modifying the control output from u to $-u$, thereby correcting the error between the heading angle and course setting.

The output of the actuator is typically:

$$u = K_p e + K_i \int e\mathrm{d}t + K_d \frac{\mathrm{d}e}{\mathrm{d}t} \tag{27}$$

When a signal reversal is detected and the feedback signal is negated, the controller output is adjusted to $u' = -u$. This modification causes the system to move in the direction opposite the setting course. However, with appropriate control strategies (such as gain adjustment), the system gradually returns to normal operation. Negating both the feedback signal and controller output enables the system to function effectively during signal anomalies, thereby enhancing robustness against attacks and disturbances while maintaining course control objectives.

3.2 Switching system design

The positive-feedback mechanism implemented in this study constitutes a mathematical dual of conventional negative–feedback systems. In standard negative-feedback-controlled architectures, the closed-loop transfer characteristic assumes the form $K'G/(1+K'G)$, where K' represents the control algorithm after incorporating nonlinear feedback. Positive feedback is achieved by changing the sign of the denominator and negating the numerator. This constitutes a fundamental equivalent transformation; hence, the controller K' can be negated by: first, converting the feedback signal from negative to positive, then multiplying the original negative feedback controller by -1 to obtain the positive feedback controller, and finally negating the system output. This process realizes an equivalent transformation between negative and positive feedbacks:

$$\frac{GK'}{1+GK'} = \frac{-G(-K')}{1-G(-K')} \tag{28}$$

The left side of Eq. (28) represents the transfer function of the negative–feedback control system, whereas the right side represents that of the positive-feedback control system. When employing a positive-feedback controller, the output of the positive-feedback system differs from that of the negative-feedback system by a negative sign. This formulation governs the control-mode switching logic during polarity inversion events, where the $-K'$ parameter configuration represents a positive-feedback operational regime. Fundamental control theory states that all negative-feedback-stabilized systems possess theoretically equivalent positive-feedback-based counterparts within their design parameter space.

3.3 Application of switched systems in collision avoidance

This controller can also be applied for ship collision avoidance. In ship motion control, when switching from a set course of 20° to a target course of 340°, conventional algorithms typically adjust based on the

difference between the target course and current heading. However, for heading changes, particularly those crossing the 0° line, conventional algorithms enable the ship to select a longer turning path, thereby prolonging the turning time.

(1) Issues with conventional algorithms:

Conventional heading-keeping control algorithms are adjusted based on angular differences in the heading. For example, if the ship's current heading is 20° and the target heading is 340°, the algorithm directly calculates the difference as follows: $\Delta\theta = 340° - 20° = 320°$. Hence, according to the conventional algorithm understanding, the ship would turn clockwise from 20° to 340°, thereby traversing a path of 320°, nearly a full circle. This extended turning time is unsuitable for situations requiring quick adjustments, such as collision avoidance.

(2) Optimization approach: converting 340° to -20°

In ship motion control, the heading angle can be viewed as circular, typically ranging from 0° to 360°. To optimize the turning path and avoid excessive turning times, the heading angle can be processed equivalently. Although ship compasses do not display negative angles, using them in control algorithms provides a convenient mathematical expression that simplifies calculations and optimizes heading-keeping control. In practice, negative angles serve as a computational tool within the algorithm to represent the angular differences in opposite directions. The specific approach is as follows.

Convert the heading angle to the minimum turning angle: The target heading of 340°can be considered as -20°. Both 340° and -20° represent the same point on the compass, which is near the northwest direction. Therefore, by processing 340° as -20° in the algorithm, we are essentially instructing the system to "rotate 40° counterclockwise." This approach optimizes the turning path, enabling an efficient and timely response to heading adjustments.

Practical controllers do not employ "turning to -20°" as an instruction; instead, they convert it into a compass-consistent command, namely "the target heading is 340°, adjust counterclockwise by 40°." This is because the clockwise angle between 340° and 20° is 320°, whereas the counterclockwise angle is only 40°. Therefore, the ship can directly adjust counterclockwise by 40° to quickly reach the target heading $340° \equiv -20°$. Therefore, the turning time was significantly reduced.

(3) Processing methods in control algorithms

Optimization of the angle-difference calculation formula: In control algorithms, the handling of heading-angle differences ensures that the ship always turns along the shortest path. The new angle-difference calculation formula can be expressed as:

$$\Delta\theta = \begin{cases} \theta_{goal} - \theta_{current}, & \left|\theta_{goal} - \theta_{current}\right| \le 180° \\ \theta_{goal} - \theta_{current} - 360°, & \theta_{goal} - \theta_{current} > 180° \\ \theta_{goal} - \theta_{current} + 360°, & \theta_{goal} - \theta_{current} < -180° \end{cases} \tag{29}$$

This optimized formula ensures that the ship always selects the shortest path during heading adjustments.

Control system optimization: Although negative angles were employed to simplify the mathematical calculations, the final output control commands adhered to the 360° representation of the compass. Therefore, while internal calculations utilize negative-angle processing, actual operations and displays are entirely based on the 0° to 360° range of the compass, ensuring that the system remains consistent with real-world compass data.

Time optimization in motion control: Through this angle-conversion process, the turning angle of the ship was significantly reduced. For example, when adjusting from 20° to 340°, the conventional algorithm requires a turn of 320°, whereas the optimized algorithm requires only a turn of 40°. Consequently, turning time is significantly reduced, particularly in scenarios requiring rapid responses, such as emergency collision

avoidance, where this optimization demonstrates a particularly outstanding performance. Fig. 6 presents a schematic flow diagram of the positive–negative feedback switching control system.

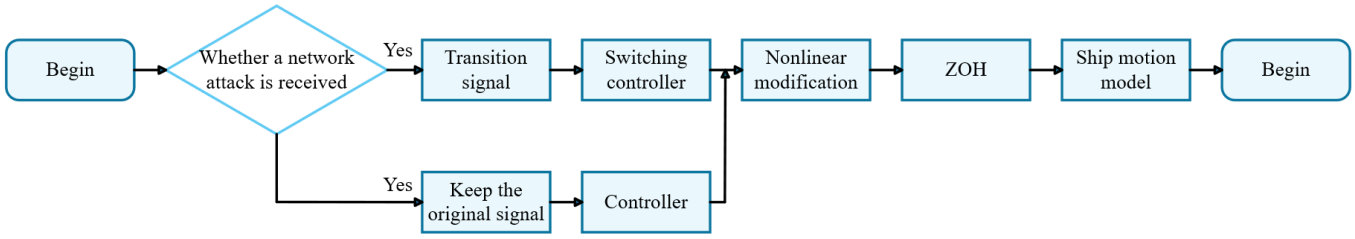

Fig. 6 Flowchart of the positive–negative feedback switching control system

4. Simulation test and result analysis

4.1 Ship parameters

The effectiveness of the control law developed in this study was validated by conducting simulations using Simulink in MATLAB. The resultant simulation framework shown in Fig. 7 emerges from the synergistic integration of the positive feedback dynamics and nonlinear compensation elements. The training ship "Yupeng" from Dalian Maritime University served as the experimental platform. Additionally, Yan [33]'s nonlinear feedback control method based on a power function, which demonstrated significant energy savings, was used as a benchmark to comprehensively evaluate the energy-saving and carbon-reduction effects of the proposed controller.

Table 1 The main particulars of "Yupeng" Ship

Name	Symbol	Unit	Yupeng
Length between perpendiculars	L	m	189.00
Breadth	B	m	27.80
Drainage volume	∇	m^3	42,293
Center of gravity	X_c	m	-1.80
Design speed	V_0	kn	17.26
Rudder area	A_R	m^2	38.00
Design draught	d	m	11.00
Block coefficient	C_b	/	0.72
Turning ability index	K_0	s^{-1}	0.38
Turning lag index	T_0	s	298.44

The following factors were assessed based on the parameters listed in Table 1: $\alpha = 18.80, \beta = 21459.9$. During the simulation, the effective working bandwidth frequency of the course-keeping controller of the ship was set as $1/3 \mathrm{rad/s}$; the design parameter was selected as $T_1 = 3\mathrm{s}$ to ensure that the closed-loop control system could effectively suppress the ocean wave frequency spectrum outside the controller's operational bandwidth. The simulation time was set to 1800 s, using the ode45 solver with variable step settings. Based on standard navigational practices, constraints on both the maximum rudder angle and maximum rudder speed were applied; the maximum rudder angle was restricted to 35°, and the maximum rudder ratio was limited to $5°/\mathrm{s}$.

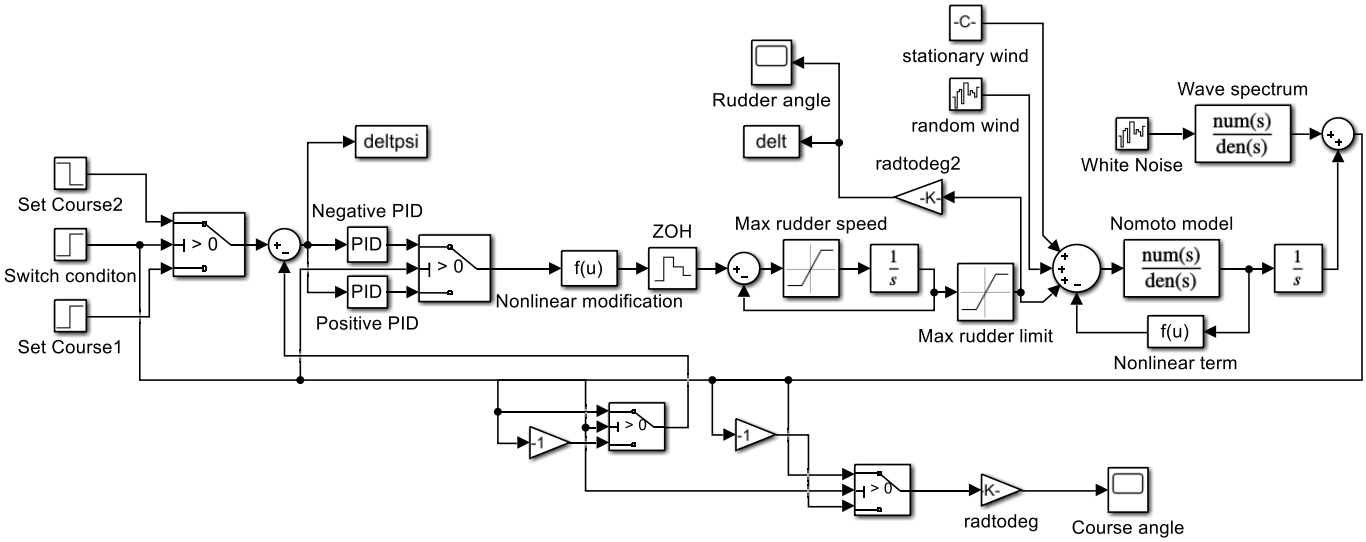

Fig. 7 Course-changing control system with ZOH based on sine nonlinear modification and CGSA

4.2 Evaluation index

The essential requirements of a controller are divided into three key characteristics: stability, accuracy, and responsiveness. In a course-keeping system, minimizing yaw error, rudder angle, and steering frequency is essential to conserve energy and reduce wear on the rudder mechanism. In this study, the yaw angle, turning time, and steering gear energy consumption serve as the principal indicators for evaluating the energy-saving performance of the controller.

Minimizing the ship yaw is critical for achieving higher speeds and reducing energy consumption. Accordingly, the maximum yaw angle ψ_m (determined by quantifying the maximum heading deviation between the actual trajectory and the prescribed course post-maneuver) and the average yaw angle $\bar{\psi}_d$ (determined by measuring the time-averaged angular discrepancy throughout navigation) were employed to evaluate the controller's performance in managing yaw.

These metrics are defined by:

$$\psi_m = \max\left|\psi_r - \psi(t)\right| \tag{30}$$

$$\bar{\psi}_d = \frac{1}{n}\sum_{t=0}^{n-1}\left|\psi_r - \psi(t)\right| \tag{31}$$

where n represents the number of time intervals.

Reducing a ship's turning time and improving responsiveness are vital for energy conservation and lowering carbon emissions [34]. To quantify the steering response of the controller, the delay time t_d (determined by quantifying the initial time interval required for the heading response to reach 80% of its target steady-state value) and settling time t_s (determined by measuring the total duration until the heading persistently remains within the predefined tolerance boundaries of the final value) were selected.

Furthermore, decreasing both the rudder angle and its rate of change of the rudder angle mitigates steering gear wear and enhances ship speed, thereby promoting energy conservation and carbon reduction. In this study, the average rudder angle $\bar{\delta}$ and the average rate of change of the rudder angle $\bar{\delta}_d$ (sampled at an interval of 0.1 s) were used as metrics to evaluate the controller's impact on the steering gear energy consumption:

$$\bar{\delta} = \frac{1}{n}\sum_{t=0}^{n-1}\left|\delta(t)\right| \tag{32}$$

$$\bar{\delta}_d = \frac{1}{n}\sum_{t=0}^{n-1}\left|\delta(t+1)-\delta(t)\right| \tag{33}$$

Based on these evaluation indices, a hierarchical model was established, with the comprehensive energy-saving index of the controller serving as the evaluation object (Fig. 8).

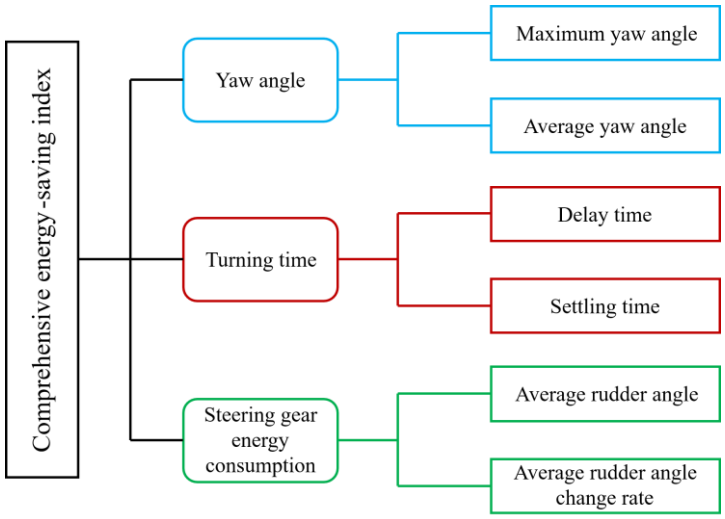

Fig. 8 Hierarchy model diagram of the comprehensive energy-saving index of the controller

4.3 Wind wave interference

In ship-maneuvering dynamics, wind and wave excitations are the dominant sources of lateral displacement (sway) and rotational deviation (yaw). To accurately simulate operational environments, the disturbance model integrates wind-induced and wave-generated perturbations, following established marine engineering principles [35]. The aerodynamic forcing is segmented into two components: steady-state wind, quantified through the wind pressure differential, and equivalent to the effective leeway angle α_{eq}. Stochastic pulsations are modeled as Gaussian white noise. The empirical relationships provided in Eq. (34) define α_{eq}:

$$\alpha_{eq} = C_w\left(\frac{V_w}{U}\right)^2 \sin(\beta_w) \tag{34}$$

where C_w denotes the wind pressure coefficient, V_w and U represent the wind velocity and ship speed, respectively, and β_w indicates the wind incidence angle. In practical implementation, this disturbance is introduced into the steering gear input as an equivalent rudder angle offset.

Adhering to ITTC protocols [36], wave excitation was simulated using white-noise-driven second-order oscillatory systems. The frequency-domain representations for Beaufort Scale conditions 6 and 8 are denoted by Eqs. (35) and Eq. (36), respectively:

$$h_1(s) = \frac{0.4198s}{s^2 + 0.3638s + 0.3675} \tag{35}$$

$$h_2(s) = \frac{1.3353s}{s^2 + 0.5153s + 0.2655} \tag{36}$$

The power spectral density functions for the wave under Beaufort Nos. 6 and 8 conditions are as follows:

$$G_{y1}(\omega)=\frac{0.1762\omega^2}{\left(0.3675-\omega^2\right)^2+0.1323\omega^2} \tag{37}$$

$$G_{y2}(\omega)=\frac{1.7608\omega^2}{\left(0.2606-\omega^2\right)^2+0.2606\omega^2} \tag{38}$$

In these equations, s represents the Laplace operator, and both the wave disturbance $h(s)$ and white Gaussian noise ω are modeled accordingly [37]. Based on the power spectral density functions in Eq. (37) and Eq. (38), three-dimensional representations of the wave interference under Beaufort Nos. 6 and 8 conditions are shown in Figs. 9 and 10, respectively.

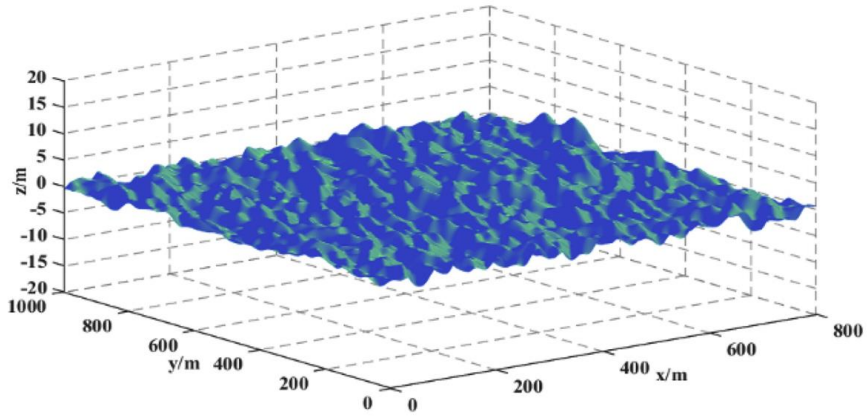

Fig. 9 Wave interference in Beaufort No.6 wind

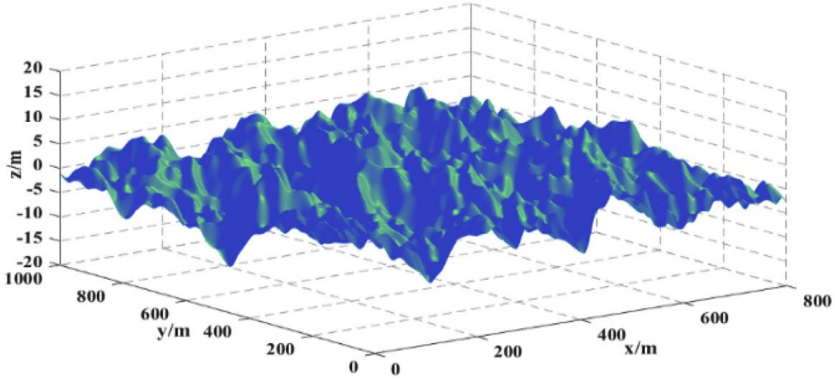

Fig. 10 Wave interference in Beaufort No.8 wind

4.4 Simulation results

During the 800-s simulation period, positive–negative signal switching was introduced into the loop to simulate network attacks on the ship. In such attacks, the hacker inverts the measurement signals. Consequently, a switching control system employing both positive and negative feedbacks was designed to address this issue. By transforming the original negative feedback system into a positive feedback configuration, the system can adapt to altered measurement signals, thereby enhancing its robustness against cyberattacks.

4.4.1 Simulation experiments in normal sea states

Under Beaufort 6 conditions, which represent a normal sea state, the proposed controller was evaluated in a course-changing scenario from 20° to 340° over 1800 s. As illustrated in Figs. 11 and 12 and listed in Table 2, the controller effectively managed the heading reversal at 800 s, exhibiting a transient overshoot

followed by rapid convergence with minimal oscillations. This demonstrates robust performance against both signal inversion–based cyberattacks and environmental disturbances.

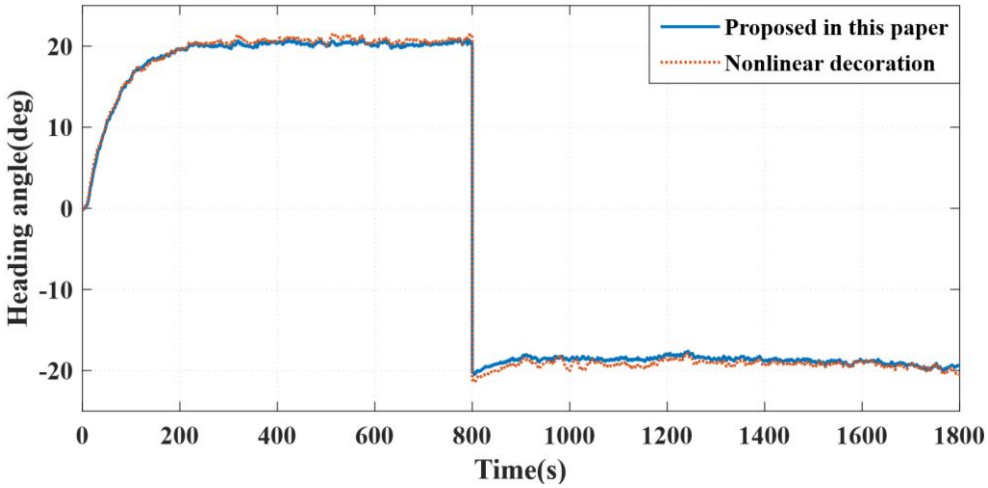

Fig. 11 Course control effects of Scenario 1

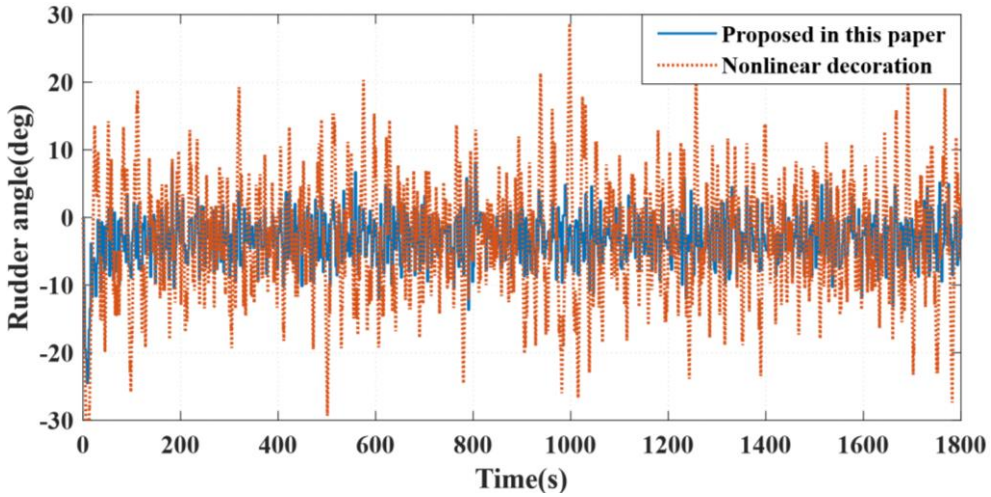

Fig. 12 Rudder angle change of Scenario 1

The quantitative results confirmed the significant advantages over the nonlinear modified benchmark. The proposed controller reduced the average and maximum yaw angles by 50.0% and 44.87%, respectively, thereby minimizing energy losses from the lateral drift. Furthermore, it achieved a 1.83% shorter delay time and a 1.51% faster settling time, indicating superior dynamic responsiveness. This rapid stabilization is attributed to the configured parameters of the nonlinear modification and the zero-order holder (ZOH). Under moderate disturbances, the ZOH hold time and nonlinear function gain were tuned to allow an aggressive response, enabling the system to utilize its full bandwidth for fast tracking while remaining resilient to wave-induced perturbations.

The actuator performance further underscores the controller efficiency, with a 43.21% lower average rudder angle and a 57.14% reduction in the rudder rate. The initial large rudder deflections during the transient phase are effectively damped because the ZOH holds the control signal; thus, it inherently filters high-frequency noise, which mitigates mechanical wear. The subsequent decline in rudder activity after stabilization directly translates to an 18.6% reduction in propulsion energy consumption. Therefore, the controller outperforms conventional controllers in normal seas by optimally balancing rapid response with high efficiency and low actuator wear.

Table 2 Comparison of performance of Scenario 1

Control method	$\psi_m(°)$	$\bar{\psi}_d(°)$	$t_d(s)$	$t_s(s)$	$\bar{\delta}(°)$	$\bar{\delta}_d(°/s)$
Nonlinear decoration	1.56	0.64	101.42	162.23	6.92	4.55
Proposed in this paper	0.86	0.32	99.56	159.78	3.93	1.95
Variable rate (%)	-44.87%	-50.00%	-1.83%	-1.51%	-43.21%	-57.14%

4.4.2 Simulation experiments in rough sea states

Under the heightened disturbance of the Beaufort 8 conditions, the controller performance adapts, revealing a deliberate and advantageous trade-off tuned by its core parameters. The results, shown in Figs. 13 and 14 and Table 3, indicate an increase in both the delay time by 8.37% and the settling time by 0.63% compared to the benchmark. This reflects performance degradation as well as a manifestation of the intrinsic coupling between the algorithm's design and the disturbance spectrum.

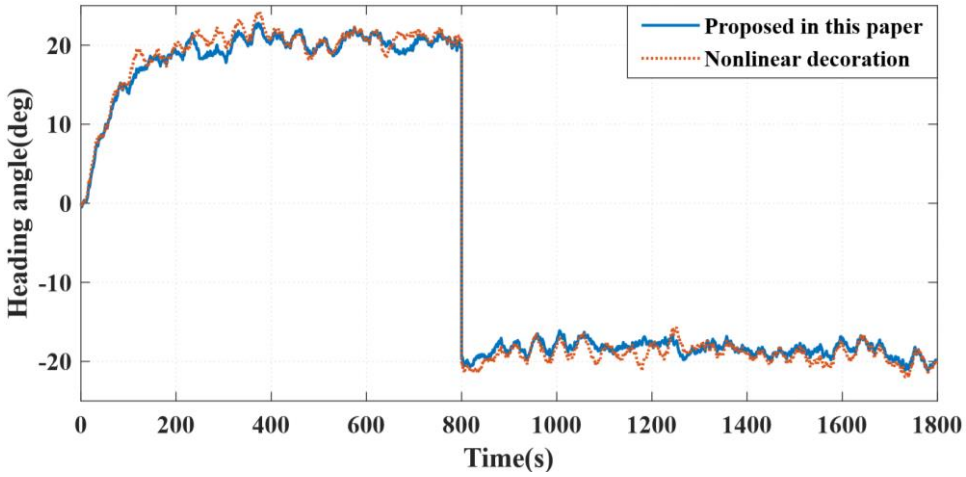

Fig. 13 Course control effects of Scenario 2

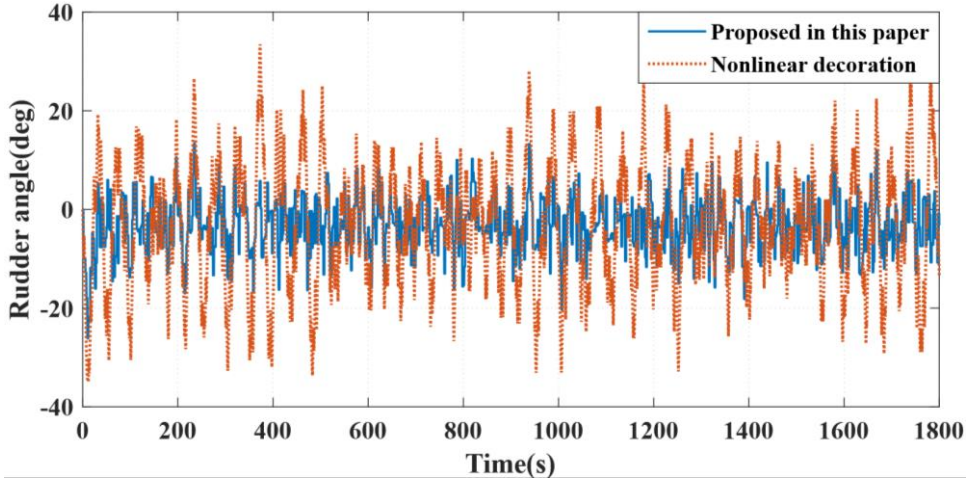

Fig. 14 Rudder angle change of Scenario 2

Table 3 Comparison of performance of Scenario 2

Control method	$\psi_m(°)$	$\bar{\psi}_d(°)$	$t_d(s)$	$t_s(s)$	$\bar{\delta}(°)$	$\bar{\delta}_d(°/s)$
Nonlinear decoration	4.25	1.05	103.02	153.28	10.03	4.68
Proposed in this paper	2.80	0.87	111.64	154.24	5.14	2.32
Variable rate (%)	-34.12%	-17.14%	8.37%	0.63%	-48.75%	-50.43%

The underlying mechanisms are as follows. The ZOH functions as a low-pass filter by maintaining a constant control signal over its sampling period. In rough seas, wave-induced disturbances contain powerful high-frequency components; therefore, a longer effective hold time, which results from the ZOH setting and the system's slows response to large disturbances, which is crucial for suppressing the control system's reaction to these high-frequency excitations and preventing excessive and counterproductive rudder motion. Consequently, control actions are inherently smoothed and slowed. Simultaneously, the nonlinear modification, whose intensity is determined by its function parameters, responds to the larger course deviations caused by severe waves and thus, tends to produce more conservative control outputs to maintain stability, further contributing to the deliberate reduction in response speed.

This disturbance coupling parameter prioritizes stability and safety over raw speed. Slower and smoother rudder movements are essential in rough seas to maintain directional control and prevent the loss of stability that can emerge from aggressive actuation. This stability-oriented strategy maintains efficiency, with the proposed controller reducing average rudder angle by 48.75% and rudder rate of change by 50.43% compared to the benchmark. Thus, the controller intelligently sacrifices marginal response speed to achieve superior actuator smoothness and energy efficiency under extreme conditions, ensuring safe and sustainable operation.

5. Simulation test and result analysis

This paper presents a robust reinforcement control method for automatic heading switching of ships based on a nonlinear modification. The experimental results confirmed a significant enhancement in the resilience of the course-changing control switching system of the ship. The proposed solution is simple, efficient, and effectively mitigates the potential risks faced by intelligent ships in complex network environments. Theoretical analysis indicates that combining nonlinear modification techniques with a ZOH can effectively reduce the output amplitude of the controller and lower the rudder frequency, thereby achieving energy saving and carbon reduction objectives. Moreover, the mathematical derivation reveals that positive feedback control is equivalent to negating both the negative feedback control law and the system output. Consequently, in the event of a cyberattack that results in inverted measurement signals, the system can automatically switch control directions. This automatic switching mechanism is significant in collision avoidance for ships, thereby enhancing their safety under unexpected network attacks. This study provides robust technical support for the navigational safety of intelligent ships, particularly autonomous vessels, by reducing control failure risks during cyberattacks and delivering significant benefits in energy conservation, carbon reduction, and reliable operation in complex environments.

Although this study demonstrates significant advancements in cyber-resilient course control under signal inversion attacks, several limitations should be acknowledged. The current framework addresses polarity reversal attacks, and its efficacy against more sophisticated cyber threats, such as false data injection, time-delay attacks, and multisensor-coordinated attacks, remains to be fully validated. Additionally, the performance of the controller was verified only under simulated Beaufort 6 and 8 conditions; testing in extreme sea states or real-world navigation environments would strengthen its practical applicability. Future work will extend the proposed architecture to address a broader spectrum of cyberattacks by integrating adaptive detection mechanisms and validating the system through full-scale sea trials. Enhancements may include introduction of machine-learning techniques for real-time attack detection and dynamic controller reconfiguration, further advancing the safety and reliability of autonomous navigation.

ACKNOWLEDGMENTS

Much appreciation to each reviewer for their valuable comments and suggestions to improve the quality of this note. This work is partially supported by the National Science Foundation of China (Grant No. 52171291, No.52571396), National Natural Science Foundation of China (No. 52201353), Doctoral Research Initial Fund Project of Liaoning Province (No. 2021-BS-078), the Fundamental Research Funds for the Central Universities (No.3132023502), the University 111 Project of China (Grant No. B08046) and International cooperation training program for innovative talents of Chinese Scholarships Council (Grant No. CSC [2022] 2260).

REFERENCES

[1] Zhou, X. Y., Liu, Z. J., Wang, F. W., Wu, Z. L., Cui, R. D., 2020. Towards applicability evaluation of hazard analysis methods for autonomous ships. *Ocean Engineering*, 214, 107773. https://doi.org/10.1016/j.oceaneng.2020.107773

[2] Zhao, H., Zhang, X., Han, X., 2019. Nonlinear control algorithms for efficiency-improved course keeping of large tankers under heavy sea state conditions. *Ocean Engineering*, 189, 106371. https://doi.org/10.1016/j.oceaneng.2019.106371

[3] Tang H, Zhu R, Wan Q., 2025. Short-term prediction of trimaran load based on data driven technology. *Brodogradnja*, 76(1), 1-26. https://doi.org/10.21278/brod76101

[4] Zhang, X. K., Han, X., Guan, W., Zhang, G. Q., 2019. Improvement of integrator backstepping control for ships with concise robust control and nonlinear decoration. *Ocean Engineering*, 189, 106349. https://doi.org/10.1016/j.oceaneng.2019.106349

[5] Cosgun T, Esenkalan M, Kinaci O K., 2024. Four-quadrant propeller hydrodynamic performance mapping for improving ship motion predictions. *Brodogradnja*, 75(3), 1-20. https://doi.org/10.21278/brod75306

[6] Shin G H, Yang H., 2025. Deep reinforcement learning for integrated vessel path planning with safe anchorage allocation, *Brodogradnja*, 76(3), 1-32. https://doi.org/10.21278/brod76305

[7] Wang, J., Xiao, Y., Li, T., Chen, C. P., 2022. Impacts of GPS spoofing on path planning of unmanned surface ships. *Electronics*, 11(5), 801. https://doi.org/10.3390/electronics11050801

[8] Liu, C., Jiang, B., Wang, X., Zhang, Y., Xie, S., 2024. Event-Based Distributed Secure Control of Unmanned Surface Vehicles With DoS Attacks. *IEEE Transactions on Systems, Man, and Cybernetics: Systems*, 54(4) 2159-2170. https://doi.org/10.1109/TSMC.2023.3341158

[9] Zhang, Y., Zhang, J., Guo, Z., Zhang, L., Shang, Y., Chen, W., 2025. The study on dynamic modeling and path planning of a manta ray-inspired underwater glider. *Brodogradnja*, 76(2), 1-35. http://doi.org/10.21278/brod76208

[10] Raman, G., Peng, J. C. H., Rahwan, T. 2019. Manipulating residents' behavior to attack the urban power distribution system. *IEEE Transactions on Industrial Informatics*, 15(10), 5575-5587. https://doi.org/10.1109/TII.2019.2903882

[11] Li, Y., Tang, Z., Gong, J., 2023. The effect of PID control scheme on the course-keeping of ship in oblique stern waves. *Brodogradnja*, 74(4), 155-178. https://doi.org/10.21278/brod74408

[12] Rødseth, Ø. J., Wennersberg, L. A. L., Nordahl, H., 2023. Improving safety of interactions between conventional and autonomous ships. *Ocean Engineering*, 284, 115206. https://doi.org/10.1016/j.oceaneng.2023.115206

[13] Zhang, H., Zhang, X., Xu, H., Soares, C. G., 2025. Cooperative path following control of USV-UAVs with genetic algorithm extended state observer. *Ocean Engineering*, 320, 120332. https://doi.org/10.1016/j.oceaneng.2025.120332

[14] Zhang, X. K., Zhang, G. Q., 2016. Design of ship course-keeping autopilot using a sine function-based nonlinear feedback technique. *Journal of Navigation*, 69(2), 246-256. https://doi.org/10.1017/S0373463315000612

[15] Ma, D., Zhang, X., Fan, J. 2024. Submarine depth and pitch control based on closed-loop gain shaping algorithm. *Journal of Marine Science and Technology*, 29, 519-528. https://doi.org/10.1007/s00773-024-01002-6

[16] Zhang, G., Lin, C., Li, J., Zhang, W., 2025. Composite anti-disturbance path following control for the underactuated surface vessel under actuator faults. *Nonlinear Dynamics*, 113(4), 3579-3592. https://doi.org/10.1007/s11071-024-10419-y

[17] Gao, S. H., Zhang, X., 2022. Course keeping control strategy for large oil tankers based on nonlinear feedback of swish function. *Ocean Engineering*, 244, 110385. https://doi.org/10.1016/j.oceaneng.2021.110385

[18] Li, G. S., Zhang, X.K., 2022. Research on the influence of wind, waves, and tidal current on ship turning ability based on Norrbin model. *Ocean Engineering*, 259, 111875. https://doi.org/10.1016/j.oceaneng.2022.111875

[19] Fan, J.M., Zhang, X., Cao, T., Ma, D., 2023. Ship longitudinal stabilization control based on CGSA and nonlinear switch modification. *Ocean Engineering*, 286, 115707. https://doi.org/10.1016/j.oceaneng.2023.115707

[20] Islam, M.M., Siffat, S.A., Ahmad, I., Liaquat, M., 2021. Robust integral backstepping and terminal synergetic control of course keeping for ships. *Ocean Engineering*, 221, 108532. https://doi.org/10.1016/j.oceaneng.2020.108532

[21] He, Z., Fan, Y., Wang, G., Qiao, S., 2023. Finite time course keeping control for unmanned surface vehicles with command filter and rudder saturation. *Ocean Engineering*, 280, 114403. https://doi.org/10.1016/j.oceaneng.2023.114403

[22] Li, G., Zhang, X., 2023. Green energy-saving robust control for ship course-keeping system based on nonlinear switching feedback. *Ocean Engineering*, 268, 113462. https://doi.org/10.1016/j.oceaneng.2022.113462

[23] Song, W., Li, Y., Tong, S., 2023. Fuzzy Finite-Time H_∞ Hybrid-Triggered Dynamic Positioning Control of Nonlinear Unmanned Marine Vehicles Under Cyber-Attacks. *IEEE Transactions on Intelligent Vehicles*, 9(1), 970-980. https://doi.org/10.1109/TIV.2023.3281578

[24] Ding, K., Zhu, Q., 2024. Network-Based Modeling and Sampling Guaranteed Cost Control for Unmanned Surface Vehicle Systems Under Stochastic Cyber-Attacks. *IEEE Transactions on Intelligent Transportation Systems*, 25(6), 6173-6185. https://doi.org/10.1109/TITS.2023.3348841

[25] Zhou, X. Y., Liu, Z. J., Wang, F. W., Wu, Z. L., 2021. A system-theoretic approach to safety and security co-analysis of autonomous ships. *Ocean Engineering*, 222, 108569. https://doi.org/10.1016/j.oceaneng.2021.108569

[26] Guo, J., Guo, H., 2023. Real-time risk detection method and protection strategy for intelligent ship network security based on cloud computing. *Symmetry*, 15(5), 988. https://doi.org/10.3390/sym15050988

[27] Zhang, X. K., Zhang, Q., Ren, H. X., Yang, G. P., 2018. Linear reduction of backstepping algorithm based on nonlinear decoration for ship course-keeping control system. *Ocean Engineering*, 147, 1-8. https://doi.org/10.1016/j.oceaneng.2017.10.017

[28] Sun, X., Wang, G., Fan, Y., 2022. Trajectory tracking control for vector propulsion unmanned surface vehicle with incomplete underactuated inputs. *IEEE Journal of Oceanic Engineering*, 48(1), 80-92. https://doi.org/10.1109/JOE.2022.3154798

[29] Shen, Z., Zhang, X., 2018. Recursive sliding-mode dynamic surface adaptive control for ship trajectory tracking with nonlinear gains. *Acta Automatica Sinica*, 44 (10), 1833–1841.

[30] Qiao, L., Zhang, W., 2020. Trajectory tracking control of AUVs via adaptive fast nonsingular integral terminal sliding mode control. *IEEE Transactions on Industrial Informatics*, 16(2), 1248–1258. https://doi.org/10.1109/TII.2019.2949007

[31] Tong, H., 2023. An adaptive error constraint line-of-sight guidance and finite-time backstepping control for unmanned surface vehicles. *Ocean Engineering* 285, 115298. https://doi.org/10.1016/j.oceaneng.2023.115298

[32] Wan, L., Su, Y., Zhang, H., Shi, B., AbouOmar, M.S., 2020. An improved integral light-of-sight guidance law for path following of unmanned surface vehicles. *Ocean Engineering*, 205, 107302. https://doi.org/10.1016/j.oceaneng.2020.107302

[33] Han, B., Duan, Z., Peng, Z., Chen, Y., 2024. A Ship Path Tracking Control Method Using a Fuzzy Control Integrated Line-of-Sight Guidance Law. *Journal of Marine Science and Engineering*, 12, 586. https://doi.org/10.3390/jmse12040586

[34] Xu, H., Guedes Soares, C., 2023. Review of Path-following Control Systems for Maritime Autonomous Surface Ships. *Journal of Marine Science and Application*, 22, 153–171. https://doi.org/10.1007/s11804-023-00338-6

[35] Kallstrom, C.G., 1982. Identification and Adaptive Control Applied to Ship Steering. Ph. D. Thesis. Lund Institute of Technology, Lund, Sweden.

[36] ITTC, 2021. Final report and recommendations to the 29th ITTC. Specialist Committee on Manoeuvring in Waves, 1 – 33.

[37] Min, B.X., Zhang, X.K., Wang, Q., 2020. Energy saving of course keeping for ships using CGSA and nonlinear decoration. *IEEE Access*, 8, 141622-141631. https://doi.org/10.1109/ACCESS.2020.3012454